remote sensing

Article

Assessment of the Feasibility of PPP-B2b Service for Real-Time Coseismic Displacement Retrieval

Hao Yang [1], Shengyue Ji [1,*], Duojie Weng [2], Zhenjie Wang [1], Kaifei He [1] and Wu Chen [3]

[1] College of Oceanography and Space Informatics, China University of Petroleum (East China), Qingdao 266580, China; upcyanghao@163.com (H.Y.); sdwzj@upc.edu.cn (Z.W.); kfhe@upc.edu.cn (K.H.)
[2] Shenzhen Research Institute, The Hong Kong Polytechnic University, Shenzhen 518057, China; ceweng@polyu.edu.hk
[3] Department of Land Surveying and Geo-Informatics, Hong Kong Polytechnic University, Hung Hom, Hong Kong 999077, China; wu.chen@polyu.edu.hk
* Correspondence: 19990045@upc.edu.cn

Abstract: Traditional coseismic displacement retrieval generally uses real-time kinematic (RTK) and precise point positioning (PPP) services. However, both RTK and real-time PPP need a network link to transmit the corrected data. Although the network link may be interrupted when an earthquake happens, the PPP-B2b service broadcasted by geostationary orbit (GEO) satellites will not be affected. Its service range mainly covers China and the surrounding areas. In this research, the PPP method with PPP-B2b service based on constrained coordinates is proposed and overcomes the limitation of the network link and long convergence time. First, the accuracy of orbits and clock offsets for the PPP-B2b service is evaluated and compared with real-time service (RTS). Then, the simulated experiments are carried out using the PPP method with PPP-B2b service based on constrained coordinates, which tests the accuracy by calculating the coordinate displacement of the measurement station. The results show that the accuracy of PPP-B2b orbits in the radial direction is within 0.1 m. Moreover, regarding the accuracy of clock offsets, the PPP-B2b service is no more than 3.5 cm. This validates the feasibility of replacing RTS products with PPP-B2b. In the 15 min simulated experiments, the root mean square (RMS) of horizontal and vertical directions is maintained within 3 cm.

Keywords: coseismic displacement; PPP-B2b; RTS; constrained coordinates

check for updates

Citation: Yang, H.; Ji, S.; Weng, D.; Wang, Z.; He, K.; Chen, W. Assessment of the Feasibility of PPP-B2b Service for Real-Time Coseismic Displacement Retrieval. *Remote Sens.* **2021**, *13*, 5011. https://doi.org/10.3390/rs13245011

Academic Editor: Athanassios Ganas

Received: 15 November 2021
Accepted: 7 December 2021
Published: 9 December 2021

Publisher's Note: MDPI stays neutral with regard to jurisdictional claims in published maps and institutional affiliations.

Copyright: © 2021 by the authors. Licensee MDPI, Basel, Switzerland. This article is an open access article distributed under the terms and conditions of the Creative Commons Attribution (CC BY) license (https://creativecommons.org/licenses/by/4.0/).

1. Introduction

Strong earthquakes cause violent crustal movements and can also trigger natural disasters, such as tsunamis, which can have a serious effect on our lives. Thus, the research of coseismic displacement retrieval is necessary. With the developments of the global navigation satellite system (GNSS), its service accuracy has become more precise, and the technical types have become varied [1–5], making it widely used in coseismic displacement retrieval and playing an important role in seismic warning [6–9]. It is also helpful for the extraction of post-earthquake information via remote sensing technology. Real-time kinematic (RTK) and real-time precise point positioning (PPP) can provide centimeter-level positioning accuracy [10–13]. However, they have some shortcomings in the application of coseismic displacement retrieval. RTK technology requires precise coordinates of reference stations, but strong earthquakes may cause the true reference coordinates to be shifted. Though real-time PPP technology can avoid the limitation of RTK [14–16], it still requires precise orbits, clock offsets, and tens of minutes to reach centimeter-level positioning accuracy [17–19]. Moreover, precise point positioning with ambiguity resolution (PPP-AR) based on uncalibrated phase delay (UPD) cannot be immune to the same problem of taking tens of minutes to converge [20,21].

In previous studies on coseismic displacement retrieval with GNSS, Colosimo et al. proposed a variometric approach for coseismic displacement retrieval based on epoch-difference phase observations, which can overcome the problem of long convergence time [22]. However, with an increase in the monitoring period, the trend of error accumulation is more obvious. Then, the linear trend removal method was used to reduce the error drift to within a few minutes, but it does not apply to scenarios where the seismic duration is more than a few minutes [23]. Li et al. proposed a temporal point positioning (TPP) method, which overcame the shortcoming of error drift in a 15 min seismic simulation test [24]. Then, the TPP method was used for retrieving the coseismic displacements of the Illapel Mw 8.3 earthquake and the Manila Trench Mw 8.0 earthquake, and the experimental accuracy using GPS/GLONASS data was better than that only using GPS data [25,26]. Weinbach et al. proposed a new PPP method that takes advantage of a highly stable oscillator connected to a GPS receiver by modeling its behavior, and coseismic vertical displacements with an amplitude of only 5 mm could be recovered [27]. Guo et al. used a modified Satellite-specific Epoch-differenced Ionospheric Delay (MSEID) model for coseismic displacement retrieval, which can obtain centimeter-level accuracy [28]. Zheng et al. developed a new approach for single-frequency precise PPP-AR with mixed single-frequency and dual-frequency receivers, and it was used for the 2018 Mw 7.9 Alaska earthquake. The accuracy of the coseismic offset estimates was about 5–7 mm [29]. Liu et al. used an alternative approach of real-time undifferenced precise positioning for testing; an accuracy of about 5 cm in the vertical could be achieved [30]. The International GNSS Service (IGS) provides a free RTS [31–33], which further improved the positioning accuracy of real-time PPP [34–37]. Some researchers used the RTS combined with the TPP method for testing [38]. However, it is still limited by the network link, and there is a risk of interruption in data communication in the seismic regions. Fortunately, the PPP-B2b service has started to be broadcast in recent years [39–41], which can provide precise corrections of real-time orbits and clock offsets after RTS interruptions. To date, no studies have used the PPP-B2b service for coseismic displacement retrieval.

Thus, this work aims to assess the feasibility of the PPP-B2b service for real-time coseismic displacement retrieval. As the service time of PPP-B2b is too short to choose suitable seismic data for experiments and, furthermore, the service area is limited to China and the surrounding area, only static data are used to demonstrate the accuracy based on simulated experiments. Firstly, the products of PPP-B2b and Centre National d'Etudes Spatiales (CNES) are used for comparison with the final precise ephemeris provided by the GeoForschungsZentrum Potsdam (GFZ) analysis center, and the accuracy of orbits and clock offsets for different services is evaluated. The feasibility of the PPP-B2b service to replace the RTS provided by CNES is demonstrated. Then, the PPP method based on constrained coordinates is used for simulated experiments with PPP-B2b, CNES, and GFZ products. To evaluate the accuracy, the coordinate displacement of the measurement station is calculated and analyzed. Finally, conclusions are summarized in the last section.

2. Methods

In this section, we first briefly introduce the correction strategy for orbit and clock offsets of the PPP-B2b service. Then, its accuracy assessment strategy is also presented. Finally, the PPP method based on constrained coordinates to perform coseismic displacement retrieval is described.

2.1. Correction Strategy for Orbit and Clock Offsets

The PPP-B2b service includes orbit and clock offset correction messages [42]. Before correcting the satellite orbits, the orbit correction messages should be transformed to the Earth-centered Earth-fixed (ECEF) coordinate system. This study applies the following formula to obtain precise satellite orbits [39]:

$$\begin{bmatrix} e_a \\ e_c \\ e_r \end{bmatrix} = \begin{bmatrix} \frac{S_v}{|S_v|} \\ \frac{S_p \times S_v}{|S_p \times S_v|} \\ e_a \times e_c \end{bmatrix} \tag{1}$$

where $[e_a\ e_c\ e_r]^T$ denotes the unit vector of satellite orbits in the along-track, cross-track, and radial directions; S_p and S_v represent the satellite orbit vector and clock offset vector computed by the broadcast ephemeris. These correction messages should be transformed to the ECEF coordinate system, and the formula can be expressed as [39]

$$dX = \begin{bmatrix} e_r & e_a & e_c \end{bmatrix} \begin{bmatrix} dR \\ dA \\ dC \end{bmatrix} \tag{2}$$

where $[dR\ dA\ dC]^T$ is the orbit correction vector in the radial, along-track, and cross-track directions; dX denotes the orbit correction vector in the ECEF coordinate system. With the broadcast satellite position X_{sat}, the precise real-time satellite position X_{apc} can be obtained by [40]

$$X_{apc} = X_{sat} - dX \tag{3}$$

Then, the precise satellite clock offset T can be obtained from the broadcast clock offset and clock offset corrections provided by the PPP-B2b service. This is calculated as follows [40]:

$$T = T_{SAT} - dT/V_C \tag{4}$$

where T_{SAT} denotes the broadcast clock offset; dT is the real-time clock offset corrections, and V_C is the velocity of light.

2.2. Assessment Strategy for Orbit and Clock Offsets

Several points of the assessment strategy for orbits need attention. Firstly, the Beidou global navigation satellite system (BDS-3) orbit correction messages provided by the PPP-B2b service are based on the antenna phase center (APC) satellite position of the B3 signal, and the GPS orbit correction messages are based on the L1/L2 ionosphere-free (IF) combination APC satellite position. However, the orbits provided by the final precise products refer to the center of mass (CoM). Hence, the satellite APC position also requires the phase center offset (PCO) corrections to be transformed to the CoM position [41]. The corrections can be expressed as

$$X_{com} = X_{apc} - A^T \cdot X_{pco} \tag{5}$$

where X_{com} denotes the satellite CoM position; X_{apc} is the satellite APC position, and A^T is the satellite attitude matrix; X_{pco} represents the PCO corrections for satellite orbits. To assess the accuracy of the orbits, single-difference values are calculated between the corrected satellite position and the precise position provided by GFZ (GBM) products. Then, its accuracy in the radial, along-track, and cross-track directions is evaluated.

For the assessment of clock offsets, the strategy is obviously more complicated than for that of orbits. Firstly, the clock offsets from the PPP-B2b service refer to the B3 signal. In contrast to the PPP-B2b service, the clock offsets from GBM products refer to the B1/B3 IF combination. Therefore, differential code bias (DCB) must be applied to clock offsets before assessment. The formula can be expressed as [41]

$$T_{IF,b1b3} = T - \frac{f_1^2}{f_1^2 - f_3^2} \cdot DCB_{b1b3} \tag{6}$$

where $T_{IF,b1b3}$ represents the clock offsets in reference to the B1/B3 IF combination; T represents the clock offsets corrected by the PPP-B2b service; f_1 and f_3 represent the B1 and B3 frequencies, respectively; DCB_{b1b3} is the inter-frequency bias between B1 and B3 frequencies. Then, the single-difference (SD) values are calculated between the corrected clock offsets and the clock offsets provided by GFZ products. Before the assessment, it must be borne in mind that a systematic bias of satellite clock offsets will affect the evaluation accuracy, so the double-difference (DD) method is used to reduce the influence of this bias [40]. The formula can be obtained by

$$\nabla\Delta T^{s}_{a,b} = (T^{s}_{a} - T^{s}_{b}) - \frac{1}{M}\sum_{i=1}^{M}\left(T^{i}_{a} - T^{i}_{b}\right) \tag{7}$$

where $\nabla\Delta$ is the DD operator; $\nabla\Delta T^{s}_{a,b}$ denotes the DD value of the clock offsets; T^{s}_{a} and T^{s}_{b} denote the clock offsets of products a and b, respectively, for satellite s; M represents the number of satellites in each epoch, and $\frac{1}{M}\sum_{i=1}^{M}\left(T^{i}_{a} - T^{i}_{b}\right)$ represents the average value of all clock offset SD values between two products. In this study, $\nabla\Delta T^{s}_{a,b}$ is used to evaluate the accuracy of the satellite clock offsets.

2.3. PPP Model Based on Constrained Coordinates

The traditional IF phase combination positioning equation can be expressed as

$$AX + BN + MZ = L \tag{8}$$

where L is the IF phase combination vector; X represents the coordinate vector; N and Z represent the phase ambiguity and zenith tropospheric delay, respectively; A, B, and M are the corresponding coefficients.

At epoch t_0, the positioning equation is expressed as

$$A(t_0)\cdot X(t_0) + B(t_0)\cdot N(t_0) + M(t_0)Z(t_0) = L(t_0) \tag{9}$$

The ambiguity (t_0) vector can be estimated as

$$N(t_0) = B^{-1}(t_0)(L(t_0) - A(t_0)X(t_0) - M(t_0)Z(t_0)) \tag{10}$$

Then, the ambiguity (t_0) vector is substituted into the equation at epoch t_i ($i > 0$):

$$A(t_i)\cdot X(t_i) = L(t_i) - B(t_i)^{-1}\cdot N(t_0) \tag{11}$$

Hence, the precise rover position at epoch t_i can be computed according to

$$X(t_i) = \left(A^{T}(t_i)P(t_i)A(t_i)\right)^{-1}A^{T}(t_i)P(t_i)\left(L(t_i) - B(t_i)^{-1}N(t_0)\right) \tag{12}$$

where $P(t_i)$ is the corresponding weight matrix. In our processing, the ambiguity (t_0) is treated as float solution, and it includes some errors not fully corrected, such as satellite ephemeris errors and tropospheric wet delay errors. However, as the variation of these errors is stable, they have no obvious influence on the accuracy of displacement inversion in a short time, such as 15 min.

3. Numerical Results

There are two numerical tests. For the first, the accuracy of PPP-B2b and CNES products is evaluated by comparing them to the GBM final products. For the second, simulation experiments on retrieving coseismic displacements are carried out with the coordinate-constrained PPP model based on PPP-B2b and CNES products; the displacements are calculated between the initial station coordinates and the subsequent epoch station position, and the displacement errors are used to evaluate positioning performance. The flowchart of the proposed algorithm is displayed in Figure 1.

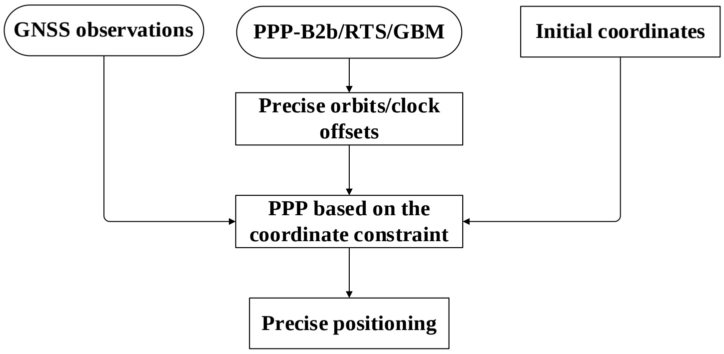

Figure 1. Flowchart of processing.

3.1. Evaluation of Orbit and Clock Offsets

The correction messages of the PPP-B2b service were collected over five days from day of the year (DOY) 187 to 191 in 2021. For the CNAV1 navigation messages of the BDS-3 B1C signal and the LNAV navigation message of GPS, the orbit and clock offset corrections were applied to obtain the precise orbits and clock offsets. Meanwhile, the real-time orbit and clock offset products of CNES in the corresponding period were downloaded (http://www.ppp-wizard.net/products/REAL_TIME/, accessed on 3 October 2021). Then, an accuracy assessment of PPP-B2b and CNES products was carried out by using GBM precise orbits and clock offsets as references. It was noted that the BDS-3 satellite messages of the PPP-B2b service only contain C19-C46, whereas CNES products only contain C19-C37. Hence, only the accuracy of the shared BDS-3 satellites of C19-C37 was assessed.

The average root mean square (RMS) values of the orbit errors for the five-day period were calculated. See Figures 2 and 3 for the detailed CNES orbit accuracy in the radial, along-track, and cross-track directions. For the BDS-3 and GPS satellites, the RMS values of the orbit errors do not exceed 0.1 m in all three directions. Meanwhile, the errors of the radial components are clearly smaller than those of the other directions, whereas the errors of the along-crack component are generally the largest. Figures 4 and 5 illustrate the BDS-3 and GPS orbit accuracies for the PPP-B2b products. The radial errors are also within 0.1 m. In contrast, the errors of the along-track and cross-track directions seem to be larger than those of the CNES products, and GPS orbit errors are no more than about 0.6 m, while most BDS-3 orbit errors are within 0.5 m. The reason may be that PPP-B2b messages are calculated using the regional network in China, whereas CNES uses a global network [41].

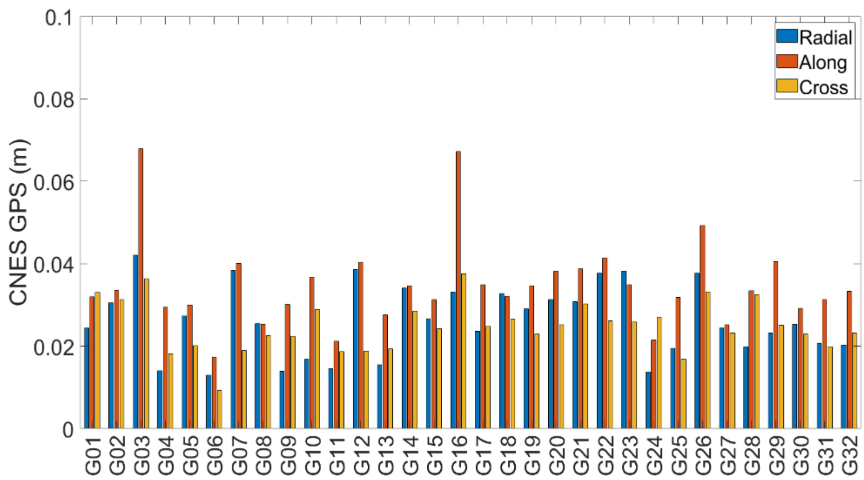

Figure 2. RMS values of GPS orbit errors for the CNES products.

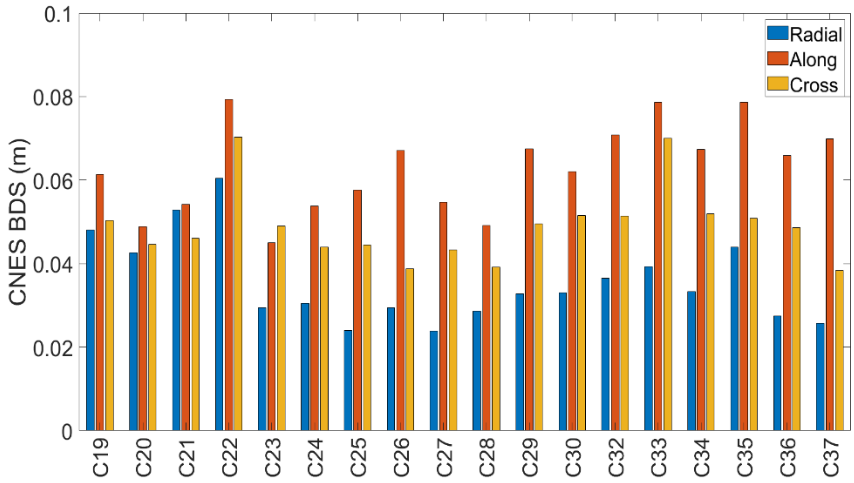

Figure 3. RMS values of BDS-3 orbit errors for the CNES products.

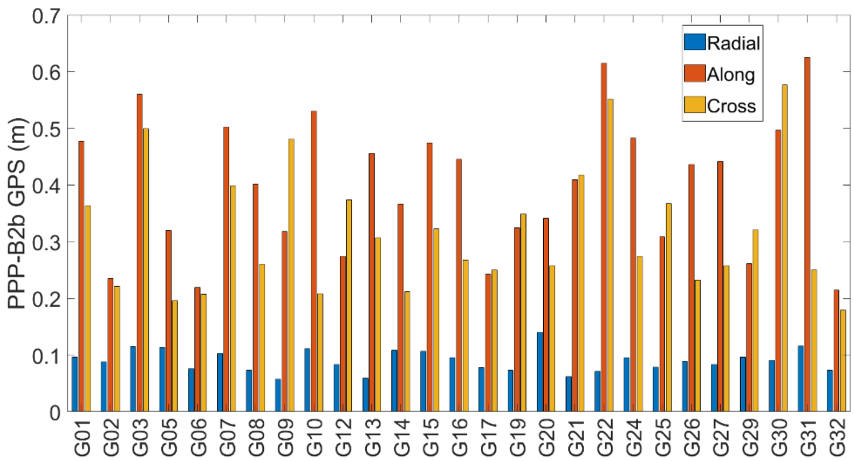

Figure 4. RMS values of GPS orbit errors for the PPP-B2b products.

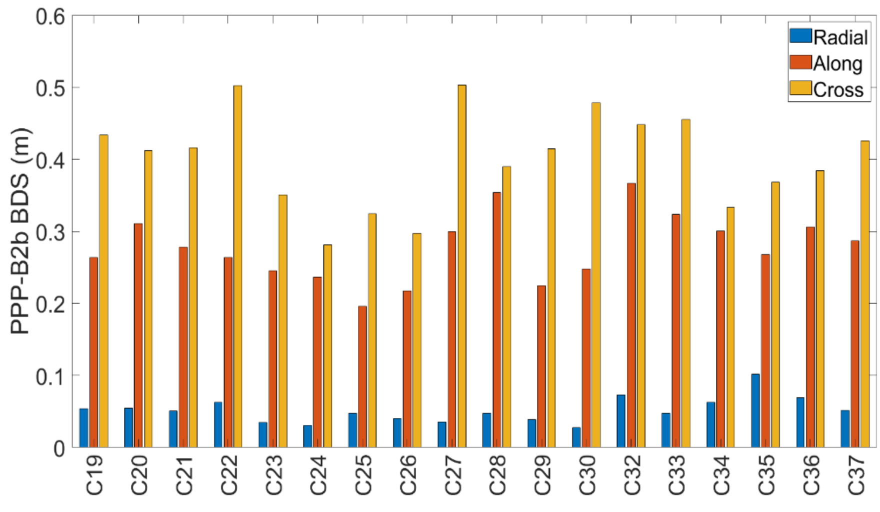

Figure 5. RMS values of BDS-3 orbit errors for the PPP-B2b products.

The evaluation strategy of clock errors is different from that of orbit errors. Since the average SD values of the satellite clock offsets were used as references, this means that changes in the number of satellites in each epoch will change the reference values and affect the accuracy of the assessment. Hence, the reference of clock offsets was smoothed to reduce the impact of changes in reference values [40]. Figures 6 and 7 display the changes in the BDS-3 and GPS clock offset errors of PPP-B2b products on day 188 of 2021. After smoothing, the changes in the clock offset error were still divided into multiple arcs due to the satellite ascending and descending. To evaluate the clock offset errors, the average of RMS and standard deviation (STD) was calculated for these arcs.

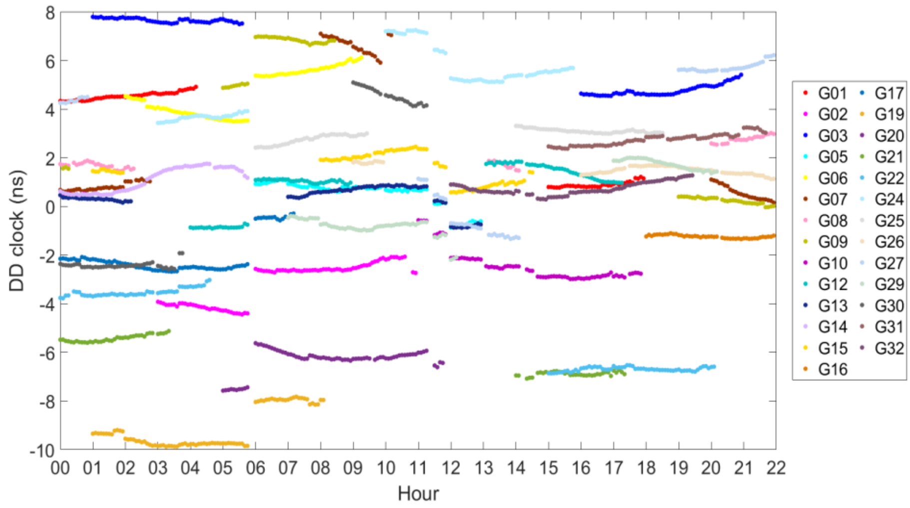

Figure 6. GPS clock offset errors for the PPP-B2b products.

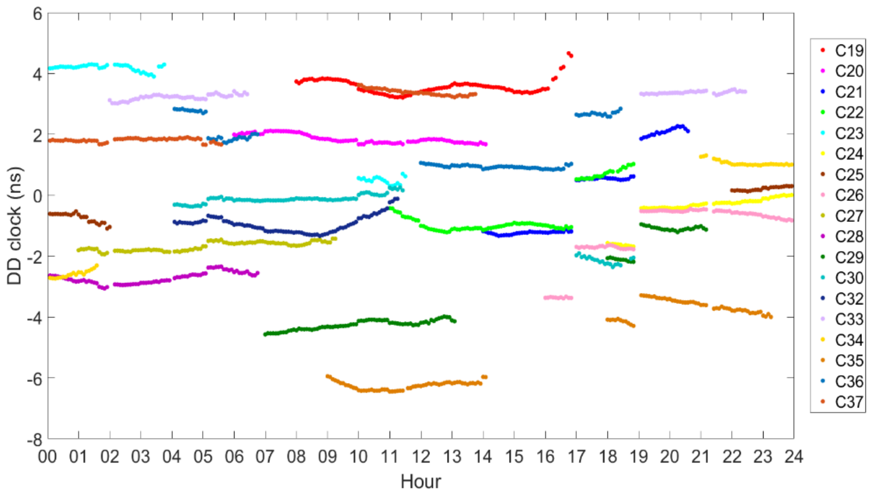

Figure 7. BDS-3 clock offset errors for the PPP-B2b products.

Figures 8–11 show the detailed accuracy of the PPP-B2b and CNES clock offset products. As the PPP-B2b service is broadcast by GEO satellites, it includes the correction messages of orbits and clock offsets, so the precise clock offsets can be calculated by combining the clock offsets of the broadcast ephemeris and the corrections of PPP-B2b. Meanwhile, there are fluctuations in the accuracy of the PPP-B2b data at different times, so the choice of data can have an impact on the evaluation accuracy. For BDS-3 clock offsets, the accuracy of PPP-B2b is better than that of the CNES products, and the STD values are generally no more than 0.1 ns. Moreover, the difference between the two products is no more than 0.05 ns. Although the RMS values of the GPS and BDS-3 clock offsets of the PPP-B2b products are about meter level, the common constant of the clock offsets will be merged into the receiver clock offset parameters when processing, which only means that the positioning accuracy will not be affected after convergence.

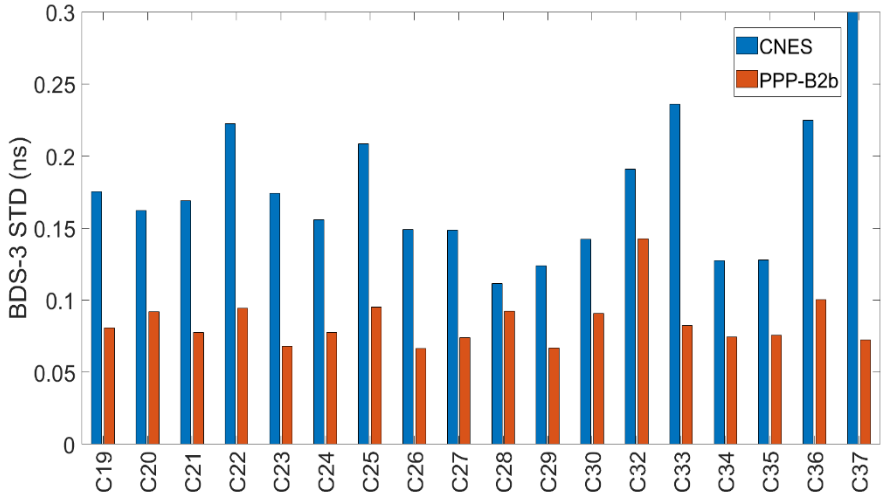

Figure 8. STD values of BDS-3 clock offset errors for the PPP-B2b and CNES products.

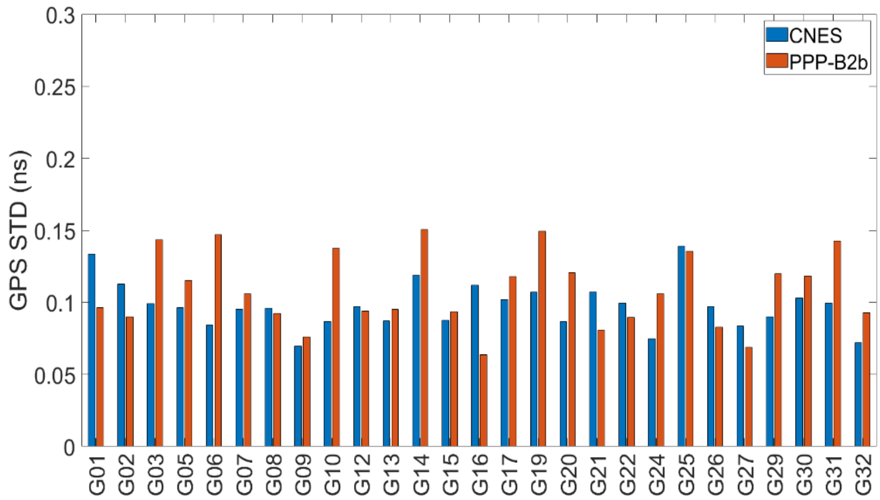

Figure 9. STD values of GPS clock errors for the PPP-B2b and CNES products.

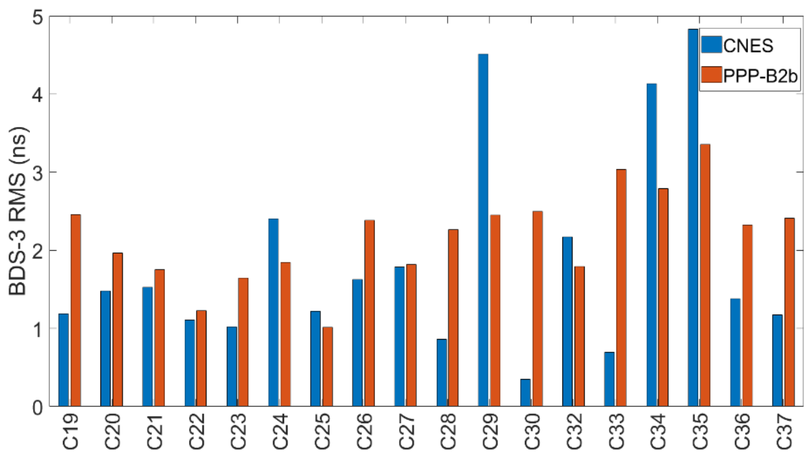

Figure 10. RMS values of BDS-3 clock errors for the PPP-B2b and CNES products.

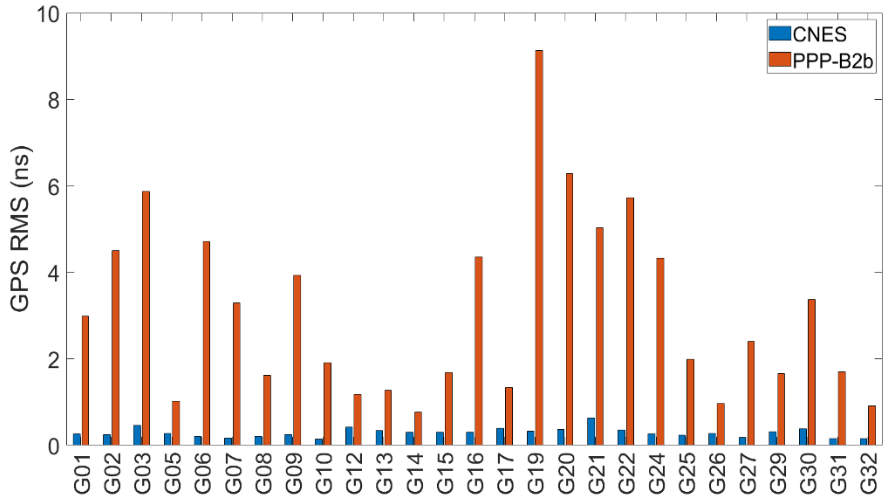

Figure 11. RMS values of GPS clock errors for the PPP-B2b and CNES products.

The average STD and RMS of the CNES and PPP-B2b orbit and clock offsets are given in Table 1. According to the statistics, the accuracy of the PPP-B2b corrections of the radial component cannot be more than 0.1 m, which is slightly worse than that of the CNES products. For the clock offset errors, the STD value of the PPP-B2b products of the BDS-3 clock offset is 0.025 m, which is better than that of the CNES products.

Table 1. The average STD and RMS of BDS-3/GPS PPP-B2b orbits and clock errors (unit: m).

Service	System	Radial	Along	Cross	Clock
PPP-B2b	BDS-3	0.077	0.314	0.422	0.025
	GPS	0.090	0.399	0.319	0.032
CNES	BDS-3	0.036	0.063	0.049	0.052
	GPS	0.026	0.035	0.025	0.029

3.2. Positioning Test

To assess the positioning performance of the PPP model based on constrained coordinates with the PPP-B2b service, the observations from JFNG and WUH2 stations in Wuhan were used in kinematic mode, and the sampling interval was 1 s. Both JFNG and WUH2 can collect GPS/BDS-3/GLONASS/GALILEO data. JFNG uses TRIMBLE ALLOY and TRM59800 for the receiver and antenna, respectively, while WHU2 uses JAVAD TRE_3 and JAVRINGANT_G5T for the receiver and antenna, respectively. The experiment time was set as 07:45:00 to 10:00:00 on 6 July 2021. Figure 12 displays the detailed position of these stations. The main reason for choosing the JFNG and WHU2 stations was that the experiment needs GPS/BDS-3/GLONSS/GALILEO high-rate observations to perform, and also due to that, the service range of the PPP-B2b signal mainly covers China and its surrounding areas. There are many stations in the PPP-B2b service area, but only JFNG and WHU2 meet the above conditions. In addition, the PPP-B2b service has recently launched, and no suitable seismic data are available. Therefore, only static data were used for simulation.

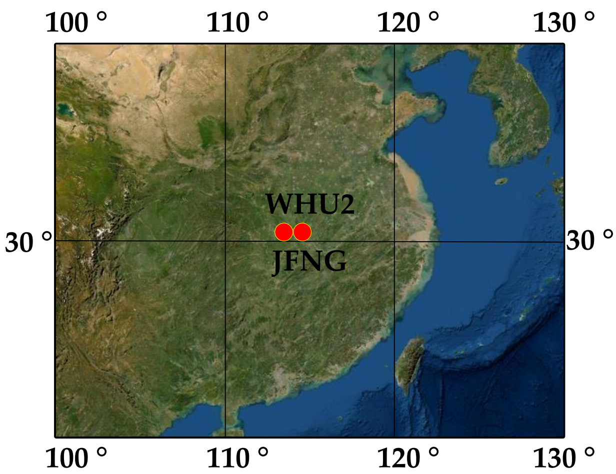

Figure 12. Position of JFNG and WHU2 stations.

The PPP method with constrained coordinates was tested with the precise orbits and clock offsets of the CNES, PPP-B2b, and GBM products. Meanwhile, the CNES and GBM products were tested with quad-system (GPS/GALILEO/GLONASS/BDS) observations, and PPP-B2b products were tested with dual-system (GPS/BDS) observations. Since ordinary seismic duration is generally no more than 15 min, the constrained period of PPP processing was set to 15 min [24], which means that each station had nine sets of experiments, and each set included three different outcomes. The precise position coordinates were computed using the Natural Resources Canada online Precise Point Positioning (CSRS-PPP) tool based on four-hour observations before the reference time (https://webapp.geod.nrcan.gc.ca/, accessed on 28 October 2021). The precise coordinates were set to initial coordinates, while the displacements between the initial coordinates and station coordinates of subsequent epochs were calculated to evaluate the positioning performance. The detailed processing strategies are shown in Table 2.

Table 2. Processing strategies.

Item	Processing Strategies
Observation type	GPS L1/L2, BDS B1/B3
Elevation mask	10°
Troposphere	Saastamoinen model
Solid tide	IERS Conventions 2010 [43]
Ocean loading	IERS Conventions 2010 [43]
Relativistic effect	Empirical model
Ambiguity	Float
PCO/Phase center variation (PCV)	IGS14.atx
Satellite orbit and clock	PPP-B2b/CNES

Figure 13 shows the positioning errors of the JFNG station, and the results of the CNES, PPP-B2b, and GBM products are represented by blue, red, and green, respectively. Note that there are nine experiments in Figure 13, with each set having a duration of 15 min. The PPP method with constrained coordinates is tested in the experiments; here, the constrained coordinates are set to the precise position coordinates, which means that the coordinate error value of the first epoch is 0. Therefore, there is not a convergence period in the figure. We can see that the horizontal accuracy is generally stable for most of the duration, and it is no more than 5 cm. In the up (U) direction, the positioning errors are a little larger, but no more than 0.1 m. The reason why the positioning accuracy of PPP-B2b is generally worse than that of the CNES and GBM products is that the CNES and GBM products have four-system data, and the number of satellites exceeds that of the PPP-B2b products.

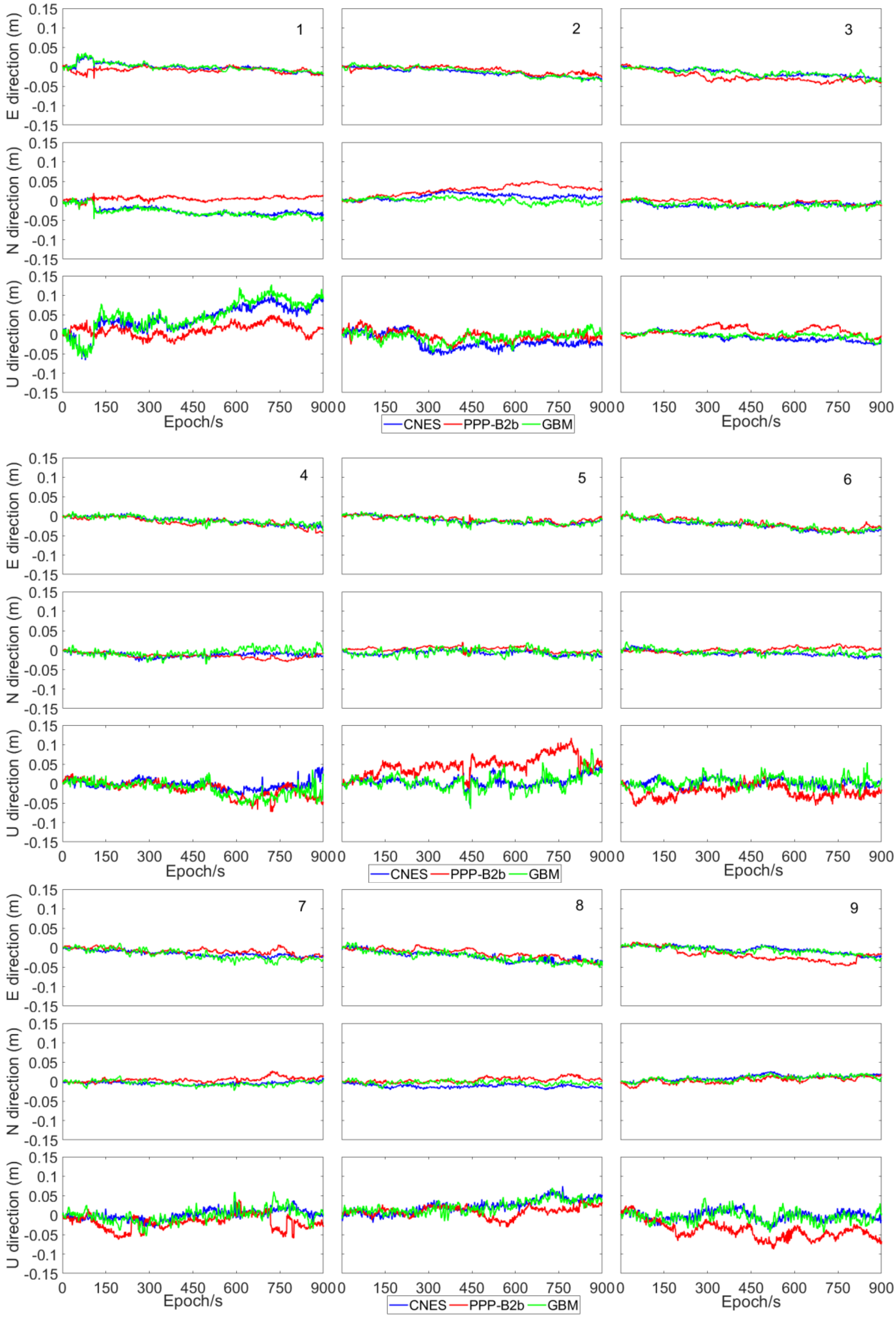

Figure 13. Positioning errors in nine sets of experiments at JFNG station.

Figure 14 shows the STD and RMS values of the positioning errors of the JFNG station in the east (E), north (N), and U directions. The RMS values are no more than 6 cm in the three directions, whereas the STD values are within 4 cm. In the U direction, the positioning accuracy of the PPP-B2b products varies greatly, while the positioning accuracies of the CNES and GBM products are similar.

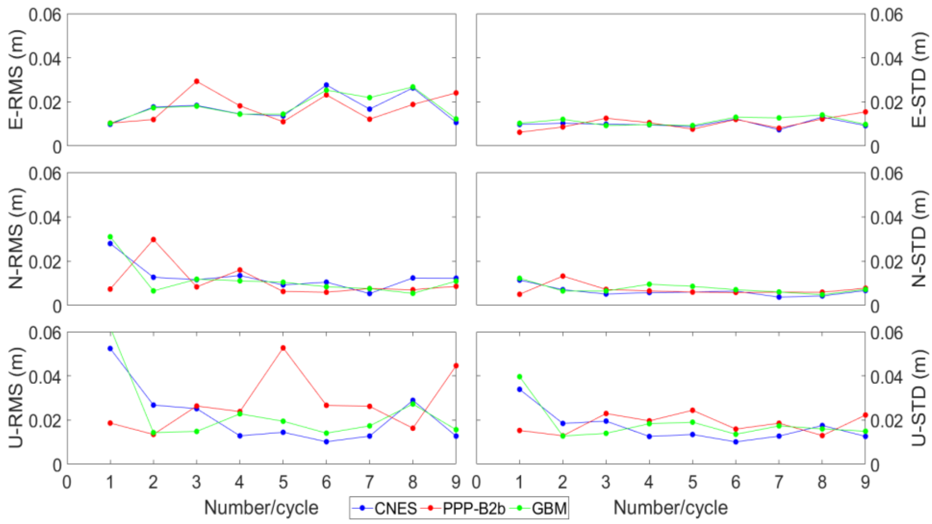

Figure 14. The STD and RMS values of positioning accuracy for JFNG station.

The positioning accuracy of the WUH2 station is shown in Figure 15. In the horizontal direction, the positioning accuracy is within 5 cm, which is similar to that of the JFNG station. Moreover, the positioning errors of the PPP-B2b products are also stable and within centimeter level in the U direction for most epochs. Although some errors of a few epochs are a little larger, they are still no more than 10 cm. From these results, we can see that the proposed method can achieve stable displacement retrieval results by using three kinds of orbit and clock offset products.

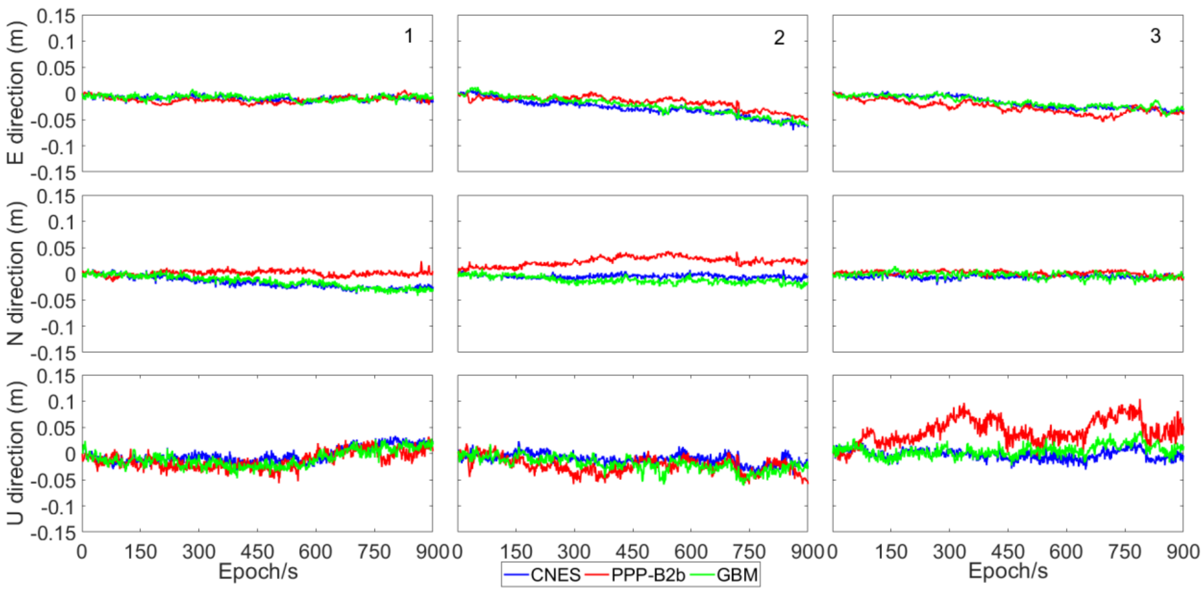

Figure 15. *Cont.*

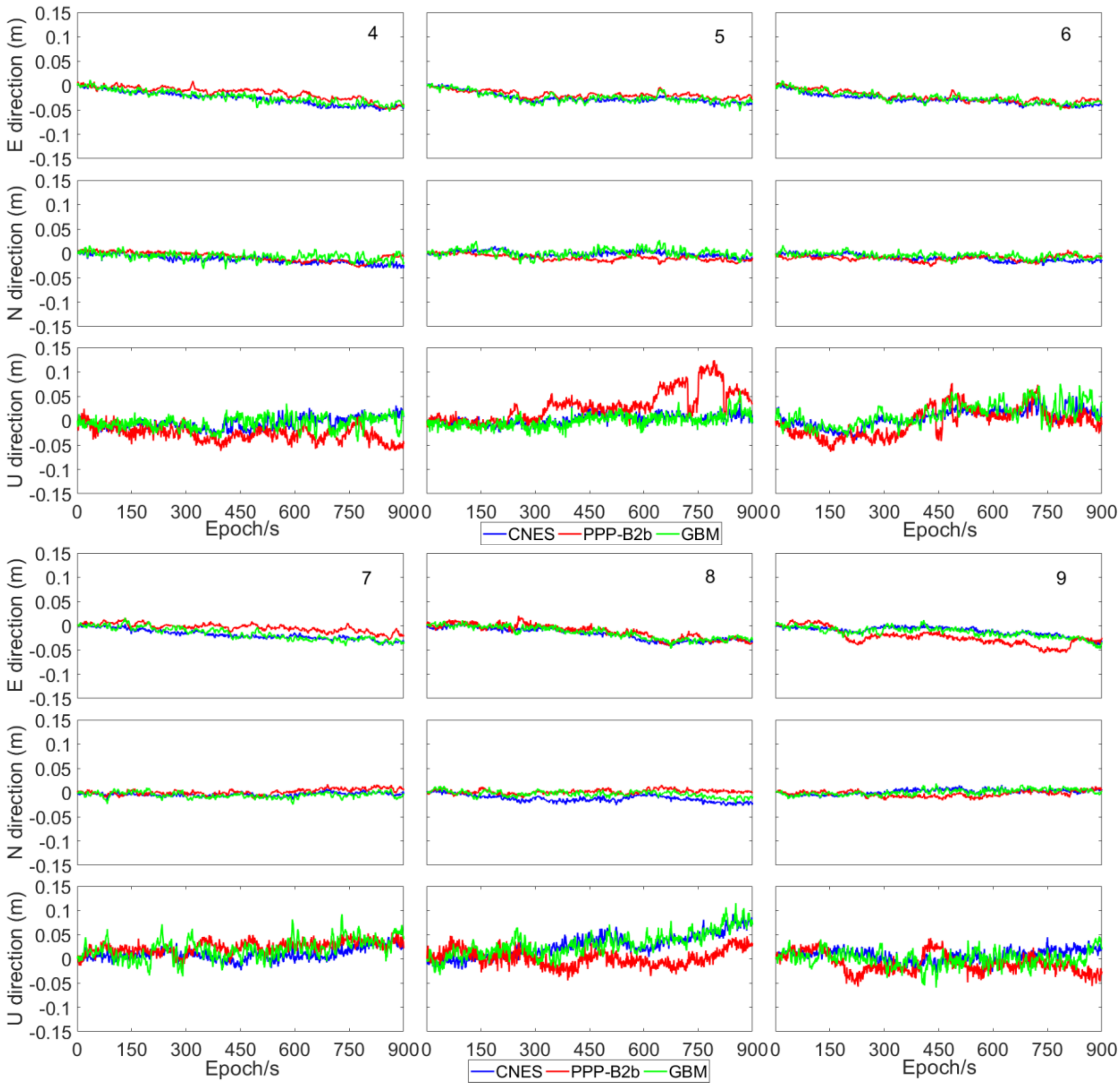

Figure 15. Positioning errors in nine sets of experiments at WHU2 station.

Figure 16 shows the STD and RMS values of the positioning solution for the WHU2 station in the E/N/U directions. The RMS values are no more than 6 cm in the three directions, while the STD values are within 4 cm. Meanwhile, the positioning results are similar to those of the JFNG station. Note that the STD and RMS values of PPP-B2b are larger than those of the CNES and GBM products in the U direction.

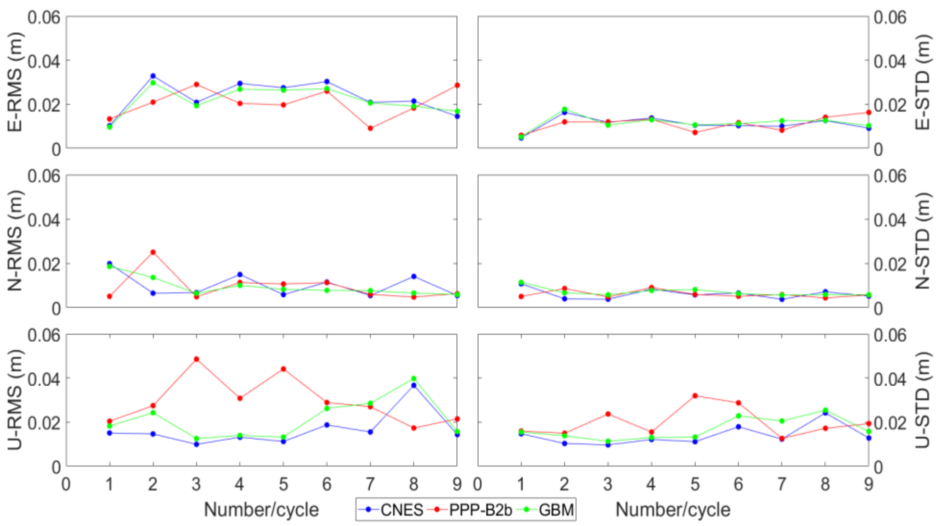

Figure 16. The STD and RMS values of positioning accuracy for WHU2 station.

To demonstrate the detailed positioning performance of the JFNG and WUH2 stations, the average STD and RMS values of the positioning errors are calculated with nine sets of experiments for each station. Table 3 further presents the positioning accuracy of JFNG and WUH2 stations, in the E direction, these performances seem to be similar when using three kinds of products, while the STD and RMS values are about 2 cm and 1 cm, respectively, and the positioning results in the N direction also have high precision. The RMS values of the PPP-B2b products in the U direction are larger than those of the CNES and GBM products, which are still no more than 3 cm. In general, the error in the vertical direction will be greater than that in the other directions. On the one hand, this is related to the quality of the data; the accuracy of the JFNG station appears to be more normal than the WHU2 station. On the other hand, this could be due to the fact that the test period is short, and when the test is extended to a day or more, the results could look more reasonable.

Table 3. The positioning accuracy of JFNG and WUH2 stations (unit: m).

Station	Type	E		N		U	
		RMS	STD	RMS	STD	RMS	STD
JFNG	PPP-B2b	0.0177	0.0104	0.0107	0.0070	0.0276	0.0183
	CNES	0.0173	0.0100	0.0128	0.0063	0.0218	0.0167
	GBM	0.0178	0.0111	0.0114	0.0076	0.0231	0.184
WHU2	PPP-B2b	0.0206	0.0112	0.0095	0.0060	0.0296	0.0200
	CNES	0.0231	0.0110	0.010	0.0061	0.0166	0.0139
	GBM	0.0217	0.0115	0.0094	0.0070	0.0214	0.0168

It was noted that the initial coordinates may affect the positioning performance of the PPP model based on constrained coordinates. In the actual coseismic displacement retrieval, the initial coordinates were computed via PPP processing with observations of previous epochs, which means that the bias between the initial coordinates and the truth-value may affect the positioning accuracy. To investigate the influence of this bias, the observations of the JFNG station with PPP-B2b products were used from 07:45:00 to 08:00:00 on 6 July 2021. The precise coordinates were obtained from PPP processing, and the errors of 0.3 m, 0.6 m, 0.9 m, and 1.2 m were manually added to the X/Y/Z direction of the precise coordinates, while the PPP method with constrained coordinates was tested with different initial coordinates in 15 min. Figure 17 shows the positioning performance with different initial coordinates. Regarding the results of this experiment, the errors can accumulate over time. The purpose of this experiment was to test whether errors in the constrained coordinates have a significant effect on positioning accuracy within a certain range. If the bias of the initial coordinates is no more than 0.4 m, the effect on the positioning accuracy is not obvious. When the bias reaches more than 0.6 m, the positioning errors in the X and Z directions remain stable, but the positioning error increases quickly in the Y direction.

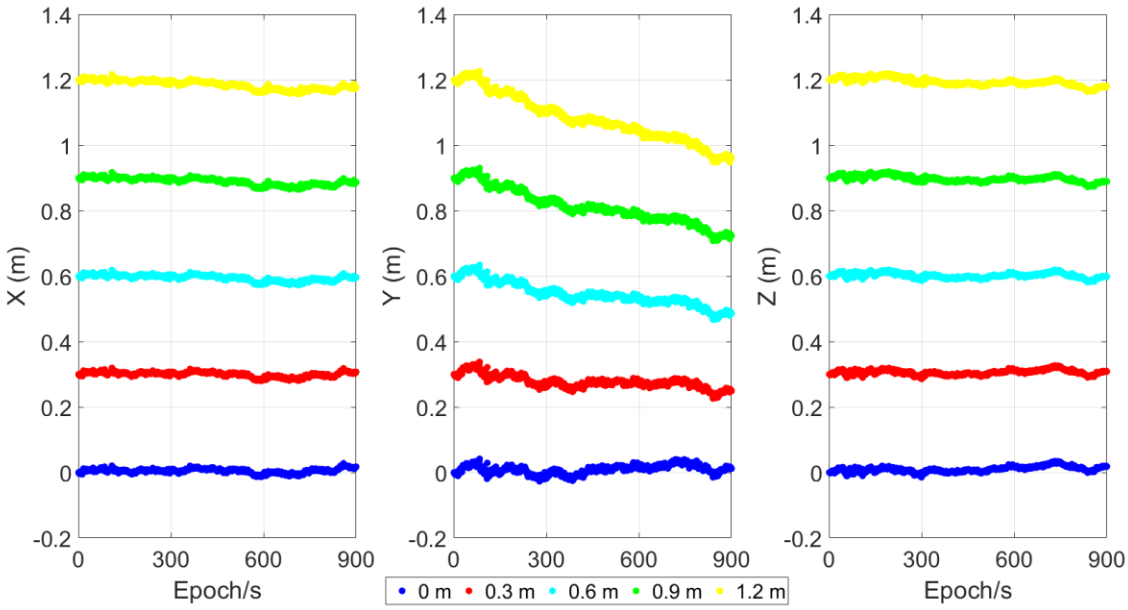

Figure 17. Positioning error in the X/Y/Z direction with different initial coordinates.

4. Discussion

In this paper, the accuracy of PPP-B2b and CNES products was evaluated and analyzed. For the PPP-B2b service, the errors of the radial components were clearly smaller than those of the other directions. Since the orbit accuracy of the radial direction has a greater impact on the positioning accuracy than the other directions, more attention was paid to the accuracy of the radial direction. The results showed that the PPP-B2b service can replace the RTS products of CNES to achieve coseismic displacement when the data communication is interrupted due to the interruption of the seismic regional network.

By using the orbits and clock offsets of PPP-B2b and CNES products, the simulated experiments were processed using static data with the PPP model based on constrained coordinates, while the displacement between the initial coordinates and the coordinates of subsequent epochs was calculated to evaluate the performance. The positioning accuracy also demonstrated that the PPP-B2B service can provide high-precision positioning results.

5. Conclusions

Previous research on coseismic displacement retrieval is almost always based on IGS real-time products and final precise products, but in this study, the PPP-B2b service was used for experiments. Firstly, the accuracy of the PPP-B2b service was evaluated and compared with that of CNES products. The experiment results validated the feasibility of replacing CNES products with PPP-B2b. Although, in general, PPP-B2b products are less accurate than CNES products, PPP-B2b receives fewer constraints from external conditions, which is its greatest advantage.

The long convergence time of the traditional PPP model was overcome by the PPP model based on constrained coordinates. Based on its performance in the simulation experiments, the positioning errors of the horizontal and vertical directions can be maintained within 3 cm, which meets the accuracy requirements of coseismic displacement retrieval. At present, the service time of the PPP-B2b signal is too short to choose suitable seismic data for testing, while the feasibility of the proposed method was verified by the simulated results with static data. Its precise positioning performance can be used to realize seismic monitoring and other applications in China and the surrounding areas.

Author Contributions: Conceptualization, H.Y. and S.J.; methodology, H.Y. and D.W.; software, H.Y. and Z.W.; validation, S.J. and K.H.; formal analysis, S.J. and W.C.; writing—original draft preparation, H.Y. and S.J.; writing—review and editing, H.Y. and S.J.; visualization, D.W. and Z.W.; supervision, K.H.; project administration, W.C.; funding acquisition, S.J., D.W., K.H., and W.C. All authors have read and agreed to the published version of the manuscript.

Funding: The research was substantially supported by the Key Program of National Natural Science Foundation of China (Grant No. 41631073) and funded by the Shenzhen Science and Technology Innovation Commission (Project No. JCYJ20170818104822282); Natural Science Foundation of Shandong Province, China (Grant No. ZR2016DM15, ZR2016DQ01, ZR2021MD060, ZR2017QD002, and ZR2017MD021); National Natural Science Foundation of China (Grant No. 41704021, 41701513, and 41604027); the Fundamental Research Funds for the Central Universities (Grant No. 18CX02064A, 18CX02054A, and 16CX02026A); and Qingdao National Laboratory for Marine Science and Technology (Grant No. QNLM2016ORP0401).

Institutional Review Board Statement: Not applicable.

Informed Consent Statement: Not applicable.

Data Availability Statement: Data included in this study are available upon request by contact with the corresponding author.

Acknowledgments: We greatly appreciate IGS and GFZ for providing multi-GNSS observation data and products.

Conflicts of Interest: The authors declare no conflict of interest.

References

1. Li, J.; Yang, Y.; He, H.; Guo, H. Benefits of BDS-3 B1C/B1I/B2a triple-frequency signals on precise positioning and ambiguity resolution. *GPS Solut.* **2020**, *24*, 100. [CrossRef]
2. Allen, R.M.; Ziv, A. Application of real-time GPS to earthquake early warning. *Geophys. Res. Lett.* **2011**, *38*, L16310. [CrossRef]
3. Gao, Z.; Li, Y.; Shan, X.; Zhu, C. Earthquake Magnitude Estimation from High-Rate GNSS Data: A Case Study of the 2021 Mw 7.3 Maduo Earthquake. *Remote Sens.* **2021**, *13*, 4478. [CrossRef]
4. Zhao, L.; Liang, R.; Shi, X.; Dai, K.; Cheng, J.; Cao, J. Detecting and Analyzing the Displacement of a Small-Magnitude Earthquake Cluster in Rong County, China by the GACOS Based InSAR Technology. *Remote Sens.* **2021**, *13*, 4137. [CrossRef]
5. Teunissen, P.J.G.; Khodabandeh, A. Review and principles of PPP-RTK methods. *J. Geod.* **2015**, *89*, 217–240. [CrossRef]
6. Shan, X.; Yin, H.; Liu, X.; Wang, Z.; Qu, C.; Zhang, G.; Li, Y.; Wang, C.; Jiang, Y. High-rate real-time GNSS seismology and early warning of earthquakes. *Chin. J. Geophys.* **2019**, *62*, 3043–3052.
7. Brack, A.; Männel, B.; Schuh, H. GLONASS FDMA data for RTK positioning: A five-system analysis. *GPS Solut.* **2021**, *25*, 9. [CrossRef]
8. Kouba, J. Measuring Seismic Waves Induced by Large Earthquakes with GPS. *Stud. Geophys. Geod.* **2003**, *47*, 741–755. [CrossRef]
9. Blewitt, G.; Kreemer, C.; Hammond, W.C.; Plag, H.P.; Stein, S.; Okal, E. Rapid determination of earthquake magnitude using GPS for tsunami warning systems. *Geophys. Res. Lett.* **2006**, *33*, L11309. [CrossRef]
10. Zumberge, J.F.; Heflin, M.B.; Jefferson, D.C.; Watkins, M.M.; Webb, F.H. Precise point positioning for the efficient and robust analysis of GPS data from large networks. *J. Geophys. Res. Solid Earth* **1997**, *102*, 5005–5017. [CrossRef]
11. Zhou, F.; Dong, D.; Li, W.; Jiang, X.; Wickert, J.; Schuh, H. GAMP: An open-source software of multi-GNSS precise point positioning using undifferenced and uncombined observations. *GPS Solut.* **2018**, *22*, 33. [CrossRef]
12. Shu, B.; Liu, H.; Xu, L.; Qian, C.; Gong, X.; An, X. Performance Analysis of BDS Medium-Long Baseline RTK Positioning Using an Empirical Troposphere Model. *Sensors* **2018**, *18*, 1199. [CrossRef]
13. Dai, L.; Eslinger, D.; Sharpe, T. Innovative algorithms to improve long range RTK reliability and availability. In Proceedings of the ION NTM, San Diego, CA, USA, 22–24 January 2007.
14. Tang, X.; Jin, S.; Roberts, G.W. Prior Position- and ZWD-Constrained PPP for Instantaneous Convergence in Real-Time Kinematic Application. *Remote Sens.* **2021**, *13*, 2756. [CrossRef]
15. Alkan, R.M.; Saka, M.H.; Ozulu, M.; İlçi, V. Kinematic precise point positioning using GPS and GLONASS measurements in marine environments. *Measurement* **2017**, *109*, 36–43. [CrossRef]
16. Xu, P.; Shi, C.; Fang, R.; Liu, J.; Niu, X.; Zhang, Q.; Yanagidani, T. High-rate precise point positioning (PPP) to measure seismic wave motions: An experimental comparison of GPS PPP with inertial measurement units. *J. Geod.* **2013**, *87*, 361–372. [CrossRef]
17. Kouba, J.; Héroux, P. Precise Point Positioning using IGS Orbit and Clock Products. *GPS Solut.* **2001**, *5*, 12–28. [CrossRef]

18. Jin, S.; Su, K. Co-seismic displacement and waveforms of the 2018 Alaska earthquake from high-rate GPS PPP velocity estimation. *J. Geod.* **2019**, *93*, 1559–1569. [CrossRef]
19. Pan, L.; Gao, X.; Hu, J.; Ma, F.; Zhang, Z.; Wu, W. Performance assessment of real-time multi-GNSS integrated PPP with uncombined and ionospheric-free combined observables. *Adv. Space Res.* **2021**, *67*, 234–252. [CrossRef]
20. Li, X.; Li, X.; Yuan, Y.; Zhang, K.; Zhang, X.; Wickert, J. Multi-GNSS phase delay estimation and PPP ambiguity resolution: GPS, BDS, GLONASS, Galileo. *J. Geod.* **2018**, *92*, 579–608. [CrossRef]
21. Banville, S.; Geng, J.; Loyer, S.; Schaer, S.; Spring, T.; Strasser, S. On the interoperability of IGS products for precise point positioning with ambiguity resolution. *J. Geod.* **2020**, *94*, 10. [CrossRef]
22. Colosimo, G.; Crespi, M.; Mazzoni, A. Real-time GPS seismology with a stand-alone receiver: A preliminary feasibility demonstration. *J. Geophys. Res. Solid Earth* **2011**, *116*, B11302. [CrossRef]
23. Branzanti, M.; Colosimo, G.; Crespi, M.; Mazzoni, A. GPS Near-Real-Time Coseismic Displacements for the Great Tohoku-oki Earthquake. *IEEE Geosci. Remote Sens. Lett.* **2013**, *10*, 372–376. [CrossRef]
24. Li, X.; Ge, M.; Guo, B.; Wickert, J.; Schuh, H. Temporal point positioning approach for real-time GNSS seismology using a single receiver. *Geophys. Res. Lett.* **2013**, *40*, 5677–5682. [CrossRef]
25. Chen, K.; Zamora, N.; Babeyko, A.; Li, X.; Ge, M. Precise Positioning of BDS, BDS/GPS: Implications for Tsunami Early Warning in South China Sea. *Remote Sens.* **2015**, *7*, 15955–15968. [CrossRef]
26. Chen, K.; Ge, M.; Babeyko, A.; Li, X.; Diao, F.; Tu, R. Retrieving real-time co-seismic displacements using GPS/GLONASS: A preliminary report from the September 2015 Mw 8.3 Illapel earthquake in Chile. *Geophys. J. Int.* **2016**, *206*, 941–953. [CrossRef]
27. Weinbach, U.; Schön, S. Improved GPS-based coseismic displacement monitoring using high-precision oscillators. *Geophys. Res. Lett.* **2015**, *42*, 3773–3779. [CrossRef]
28. Guo, B.; Zhang, X.; Ren, X.; Li, X. High-precision coseismic displacement estimation with a single-frequency GPS receiver. *Geophys. J. Int.* **2015**, *202*, 612–623. [CrossRef]
29. Zheng, K.; Zhang, X.; Li, X.; Li, P.; Sang, J.; Ma, T.; Schuh, H. Capturing coseismic displacement in real time with mixed single- and dual-frequency receivers: Application to the 2018 Mw7.9 Alaska earthquake. *GPS Solut.* **2019**, *23*, 9. [CrossRef]
30. Liu, Z.; Yue, D.; Huang, Z.; Chen, J. Performance of real-time undifferenced precise positioning assisted by remote IGS multi-GNSS stations. *GPS Solut.* **2020**, *24*, 58. [CrossRef]
31. Elsobeiey, M.; Al-Harbi, S. Performance of real-time Precise Point Positioning using IGS real-time service. *GPS Solut.* **2016**, *20*, 565–571. [CrossRef]
32. Hadas, T.; Bosy, J. IGS RTS precise orbits and clocks verification and quality degradation over time. *GPS Solut.* **2015**, *19*, 93–105. [CrossRef]
33. Abdelazeem, M.; Çelik, R.; El-Rabbany, A. An Enhanced Real-Time Regional Ionospheric Model Using IGS Real-Time Service (IGS-RTS) Products. *J. Navig.* **2016**, *69*, 521–530. [CrossRef]
34. Wang, L.; Li, Z.; Ge, M.; Neitzel, F.; Wang, X.; Yuan, H. Investigation of the performance of real-time BDS-only precise point positioning using the IGS real-time service. *GPS Solut.* **2019**, *23*, 66. [CrossRef]
35. Yang, F.; Zhao, L.; Li, L.; Feng, S.; Cheng, J. Performance Evaluation of Kinematic BDS/GNSS Real-Time Precise Point Positioning for Maritime Positioning. *J. Navig.* **2019**, *72*, 34–52. [CrossRef]
36. El-Diasty, M.; Elsobeiey, M. Precise Point Positioning Technique with IGS Real-Time Service (RTS) for Maritime Applications. *Positioning* **2015**, *6*, 71–80. [CrossRef]
37. Nie, Z.; Gao, Y.; Wang, Z.; Ji, S.; Yang, H. An approach to GPS clock prediction for real-time PPP during outages of RTS stream. *GPS Solut.* **2018**, *22*, 14. [CrossRef]
38. Zhang, Y.; Nie, Z.; Wang, Z.; Wu, H.; Xu, X. Real-Time Coseismic Displacement Retrieval Based on Temporal Point Positioning with IGS RTS Correction Products. *Sensors* **2021**, *21*, 334. [CrossRef]
39. Nie, Z.; Xu, X.; Wang, Z.; Du, J. Initial Assessment of BDS PPP-B2b Service: Precision of Orbit and Clock Corrections, and PPP Performance. *Remote Sens.* **2021**, *13*, 2050. [CrossRef]
40. Tao, J.; Liu, J.; Hu, Z.; Zhao, Q.; Chen, G.; Ju, B. Initial Assessment of the BDS-3 PPP-B2b RTS compared with the CNES RTS. *GPS Solut.* **2021**, *25*, 131. [CrossRef]
41. Xu, Y.; Yang, Y.; Li, J. Performance evaluation of BDS-3 PPP-B2b precise point positioning service. *GPS Solut.* **2021**, *25*, 142. [CrossRef]
42. China Satellite Navigation Office. BeiDou Navigation Satellite System Signal in Space Interface Control Document Precise Point Positioning Service Signal PPP-B2b (Beta Version). Available online: http://www.beidou.gov.cn/xt/gfxz/201912/P020191227331847498839.pdf (accessed on 30 September 2020).
43. Petit, G.; Luzum, B. *IERS Conventions (2010)*; Bureau International Des Poids et Mesures Sevres: Frankfurt am Main, Germany, 2010.